***Manuscript refereed by Chairman Name (Company, Country)***

# Computational Modelling of Water Sprays in Molten Metal Atomization Process

Ali Asgarian (University of Toronto, 184 College St, Toronto, ON M5S 3E4, Canada) ali.asgarian@utoronto.ca; Martin Heinrich (TU Bergakademie Freiberg, Julius-Weisbach-Bau Lampadiusstrasse 4, 09599 Freiberg, Germany) Martin.Heinrich@imfd.tu-freiberg.de; Kinnor Chattopadhyay (University of Toronto, 184 College St, Toronto, ON M5S 3E4, Canada) kinnor.chattopadhyay@utoronto.ca; Markus Bussmann (University of Toronto, 5 King's College Road Toronto, ON M5S 3G8, Canada) bussmann@mie.utoronto.ca

## Abstract

A combined physical-computational modelling approach has been developed to analyse flat fan water sprays that are widely used in water atomization of metals, where a molten metal stream is impinged by a number of high-pressure water sprays. Due to the energy transfer at the impingement zone, the molten metal stream breaks up into droplets that ultimately become powder. In this study, a lab-scale setup was built to carry out high-speed imaging of a high-pressure, but low flowrate, spray. Since analysis of an industrial-size spray is not practical in the lab, a computational fluid dynamics (CFD) model was also developed, to scale the analysis to industrial size. The CFD model combines an instability analysis of a liquid sheet and a secondary break up model of a moving droplet. An open source CFD solver, OpenFOAM, was used and some modifications were made to suit this specific subject. The results of the CFD model are compared with experimental results and some suggestions for future studies are made.

## Introduction

Powder metallurgy (PM) is a state-of-the-art technology for producing net-shape (or near net-shape) metal parts from metal powder. The PM industry has continuously grown since the 1980s and replaced conventional metal forming processes such as casting, forging, and machining in many production lines. The main advantages of PM are net-shape production, energy efficiency, porosity control, cost effectiveness, and flexibility in part design. Because of these features, PM is regarded as intrinsically sustainable compared with other technologies [1].

Looking back to the 1980s, PM manufacturing techniques encompassed hot forging/forming of powder preforms, cold forging of sintered preforms, injection molding and sintering of metal powder-plastic mixtures (MIM), and high temperature sintering (over 1200 °C) [2]. However, the market acceptance of PM was not as wide as it is today. With improvements in the early processes and emergence of new techniques such as hot/cold isostatic pressing (HIP/CIP) and metal additive manufacturing (AM), the industry has entered a new era [3]. The rapid growth of metal 3D printing and other PM processes is increasing the demand for higher-quality powders with more predictable and controlled particle morphology and size distribution.

The main route for high volume metal powder production is water atomization, that allows the production of powders up to a yield limit of about 500 kg/min for a single nozzle [4]. It is also accepted by the industry as the least expensive method. A wide range of ferrous and non-ferrous metal powders can be produced using water atomization. This includes (but is not limited to) iron, low alloy and stainless steel, copper, copper alloys, nickel-base alloys, and zinc. In this process, molten metal is poured into an atomization chamber and impinged by high-pressure water sprayed from flat fan nozzles. A flat fan nozzle generates a flat thin sheet of water that, due to an aerodynamic instability, rapidly disintegrates into a fan-shape spray. Industrial water atomizers commonly operate at water pressures ranging from 5 to 20 MPa (~750 to 3000 psi). At these high pressures, a spray is formed at a short distance from the nozzle outlet, and these high-speed water droplets continuously impinge on the surface of the melt stream and atomize it into molten metal droplets. The metal droplets then solidify to powder. It seems likely that there is a relation between the water droplet size and velocity distribution, and the as-atomized powder size distribution.

Previous research in this field has focused on finding relations between the inputs and outputs, with no concern for the intermediate thermofluidic and physicochemical phenomena. For example, owing to the scalability of the water atomization process, many empirical correlations have been developed linking the mass median particle size ($d_{50}$) to different operational parameters such as water pressure $P_W$, water velocity $V_W$, and nozzle apex angle α. Persson et al. [5] recently published a comprehensive review of existing models for powder median size. They point out in their final discussion that existing models in the literature are mainly empirical, lacking thorough understanding of complex phenomena within the atomization chamber. The long-term goal of the current research is to gain insight on the phenomena internal to the atomization chamber, including the formation of the water spray and its characteristics. Asgarian et al. [6] simulated the water spray using the built-in flat-fan spray model of ANSYS/FLUENT, a commercial CFD software. In this study, we present a flat-fan spray solver developed using the OpenFOAM platform. The spray module was used to simulate flat fan water sprays at different pressures, and these results are compared with experiments.

## Numerical Approach

The numerical model is based on the Euler-Lagrange approach to model the two-phase air-droplet flow. For this approach, the liquid jet and its transition to spray is not resolved. Instead, the breakup of the liquid sheet is computed in terms of the atomization and secondary breakup of discrete droplets into smaller ones. The atomization model is based on the instability theory for a 2D viscous liquid sheet subject to periodic disturbing waves proposed by Senecal et al. [7]. Once the liquid sheet disintegrates into parent droplets, these droplets are subject to aerodynamic forces resulting in further breakdown into child droplets [8]. This effect is simulated using the KHRT breakup model proposed by Beale and Reitz [9]. The geometric parameters of the spray, e.g. the spray spreading and dispersion angles (see Figure 3), and the flow rate are taken from experimental measurements.

The computational domain consists of a rectangular box with dimensions 50 x 180 x 200 mm as shown in Figure 1(a). The lateral boundaries are defined as atmospheric, with non-reflecting boundary conditions for pressure, to reduce the influence of reflecting pressure waves. Boundary conditions for velocity and turbulent quantities are treated as zero gradient. The mesh consists of about 1.5 x $10^6$ cells and is refined in the spray region; see Figure 1(b). The smallest cell size close to the core of the jet is about 0.8 mm. The mesh becomes gradually coarser towards the boundaries of the domain, with a maximum cell size of 6 mm. The injection point for the spray is located 1 mm below the top boundary and points in the positive z-direction. The droplet size distribution is evaluated in a plane 110 mm below the point of injection.

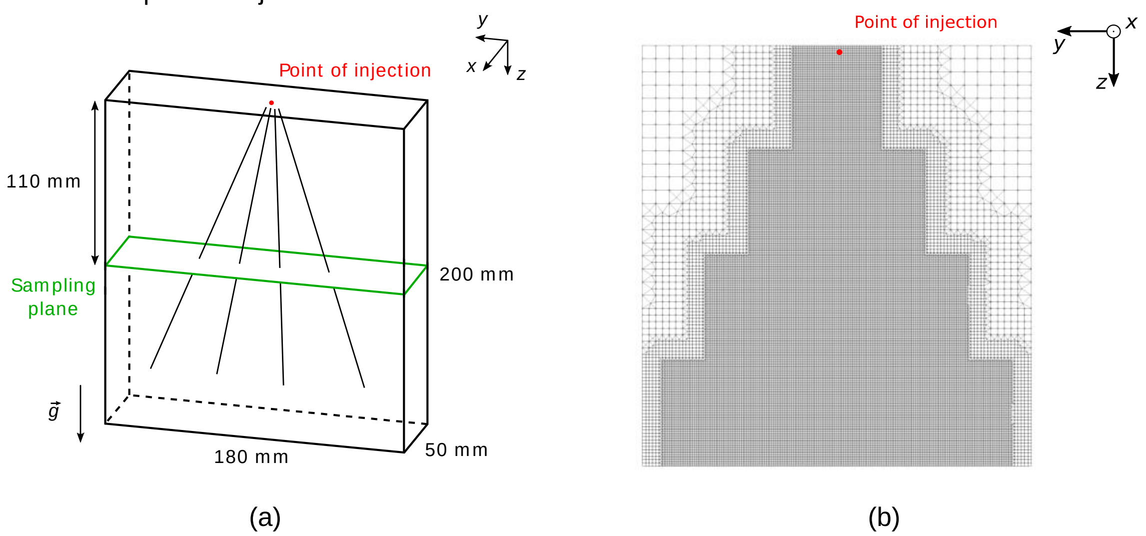


Figure 1. (a) Computational domain (b) Cross section of computational mesh

We employ the open source CFD library OpenFOAM version 5.0 [10] for the numerical simulations. The solver is based on the PIMPLE pressure-velocity coupling for transient flows. The temporal resolution is $10^{-5}$ s with a second-order backward differencing scheme. The spatial discretization is second-order upwind for the convective terms and second-order linear for the gradient terms. The k-ε turbulence model is employed. The air is considered as a perfect gas, with Sutherland's law for viscosity modelling.

## Experimental Setup

The experimental setup, see Figure 2, includes a high-pressure positive displacement pump, water conveying piping and hoses, a flat fan spray nozzle, and a transparent enclosure. In addition, a high-speed camera and a back light are used to capture shadowgraphs of the spray. High-speed images are obtained at different spray pressures and distances from the nozzle. The images are postprocessed using ImageJ, an open-source image processing software, to obtain the spreading and dispersion angles of the spray and droplet size distribution. The two characteristic angles of the spray are used to setup the CFD model, while the droplet size distribution is a means of verifying the numerical results.

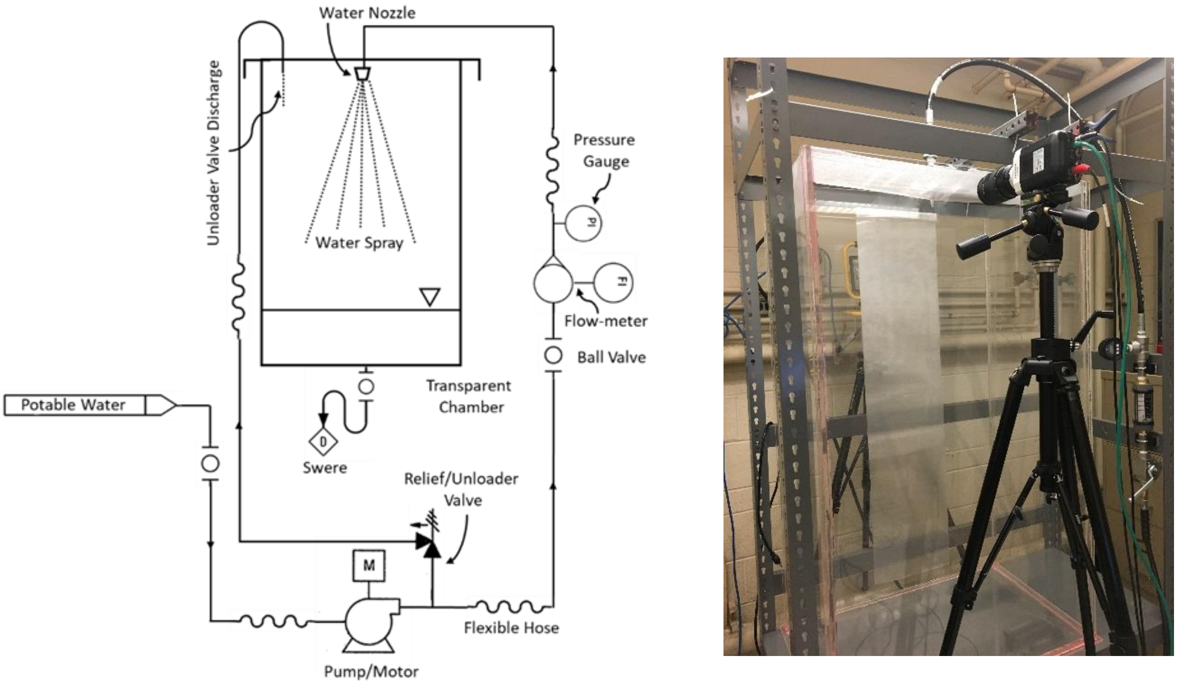


(a) (b)

Figure 2. (a) Flow diagram and (b) photo of the experimental setup

### Results

The experimental and numerical results for a 2,068 kPa (300 psi) water spray are presented in this section. The spray emerges from a flat fan nozzle; the nozzle specifications are listed in Table 1.

Table 1. Nozzle specifications

| Nozzle type | Hydraulic diameter, $D_h$ (mm) | Flowrate at 300 kPa (Lit/min) | Flowrate at 10,000 kPa (lit/min) | Spreading angle (degree) |
|---|---|---|---|---|
| Flat Fan Spray | 1.16 | 1.6 | 9.1 | 25* |

* This is a vendor published value; however, the spreading angle varies with pressure.

Figure 3 shows the first 50 mm of the spray. The breakup of the water sheet into transverse ligaments is clearly seen in Figure 3(a). Some droplets have already formed at the edge of the spray where aerodynamic drag is at its maximum. Figure 3(b) shows the emergence and growth of disturbing waves in the initial water sheet. These waves are responsible for breaking up the water sheet. This is an antisymmetric or sinuous disturbance. The spreading angle, β, and dispersion angle, θ, are 39.8° and 5.6°, respectively.

The water flowrate and spray angles were used to set up the CFD model to simulate the spray. The simulated water spray is shown in Figure 4 with the droplets coloured by their corresponding diameter. The largest droplets are directly downstream of the injection point. Once the primary breakup occurs, the droplet diameter reduces significantly to 200-250 µm. Secondary breakup occurs primarily at the edges of the spray, where the smallest droplets can be found. This effect can be attributed to aerodynamic forces being largest in this region. The largest droplets are in the core of the spray with up to 300 µm.

Figure 5 shows the droplet size distribution obtained by the CFD model at 110 mm below the nozzle. The arithmetic mean diameter is 238 µm with a maximum diameter of up to 325 µm. Figure 6(a) shows a shadowgraph of the same spray at 80 to 110 mm below the nozzle. For the sake of consistency, post-processing was done on the bottom portion of this image, 105 to 110 mm.

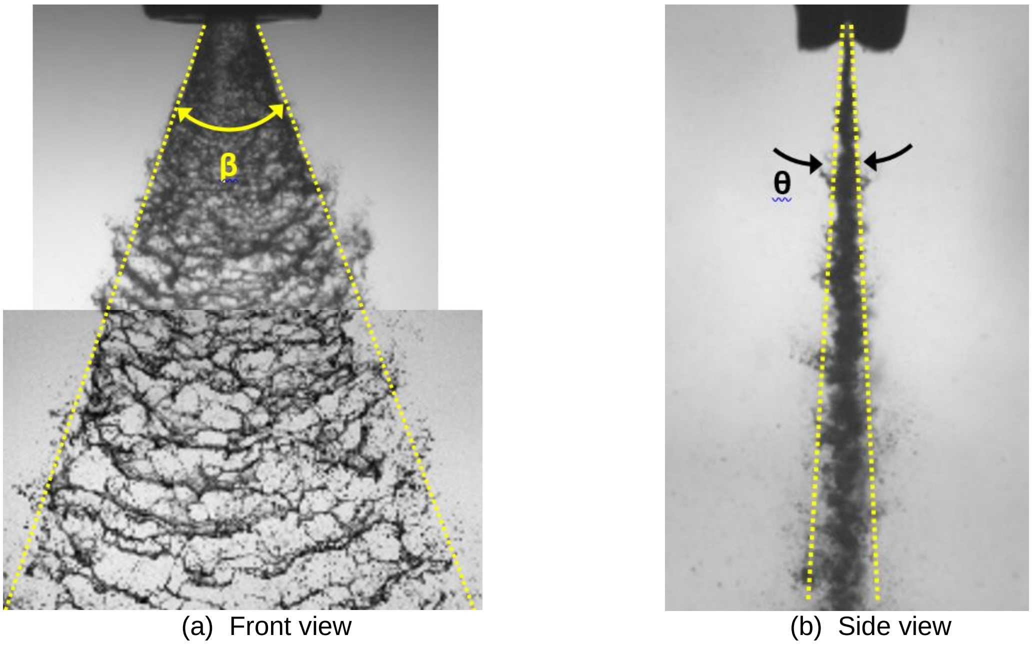


Figure 3. Spray spreading angle, β, and dispersion angle, θ, are shown from (a) front view and (b) side view of a 2,068 kPa water spray; 0 to 50 mm below the nozzle. For this spray, β and θ are 39.8° and 5.6°, respectively.

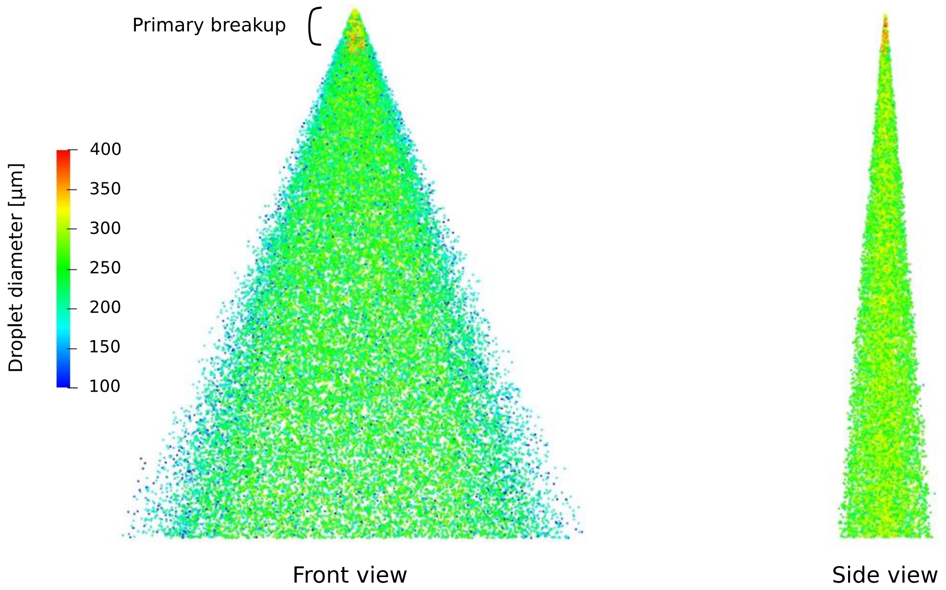


Figure 4. Numerical simulation of the spray breakup at 2,068 kPa (300 psi). The visual droplet size is overstated for presentability.

Figure 6(b) presents the image processing steps including, from top to bottom, cropping, applying a FFT filter, applying a threshold, and measuring droplets. The corresponding droplet size distribution histogram is illustrated in Figure 7. Comparing the CFD result with the experimental measurements suggests that the CFD result is narrower. This difference may be caused by the atomization model, which was originally developed for pressure-swirl atomizers. A strong turbulence in a flat fan nozzle could induce stronger breakup than predicted. A different model for secondary break up may also yield more accurate results. Further investigation on this topic is ongoing. Once the CFD model is further refined and reasonable accuracy is obtained, it will be used to predict the droplet size and velocity distribution for water sprays in an industrial-size water atomization plant.

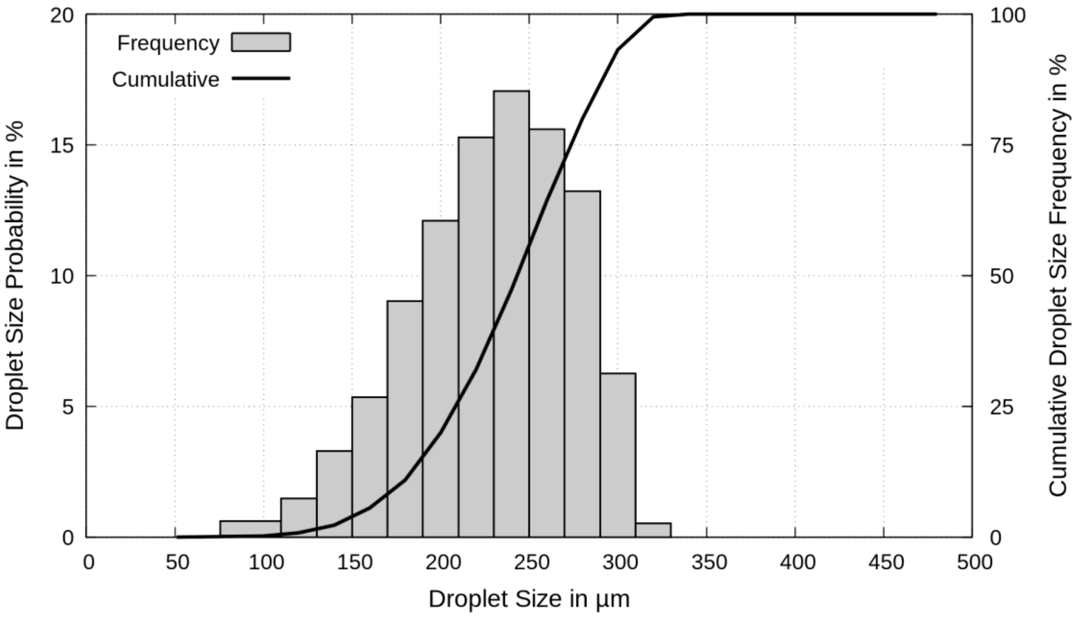


Figure 5: Numerical results for droplet size distribution for the spray at 2,068 kPa (300 psi) 110 mm below the nozzle. Arithmetic mean diameter ($d_{10}$) = 238 µm.

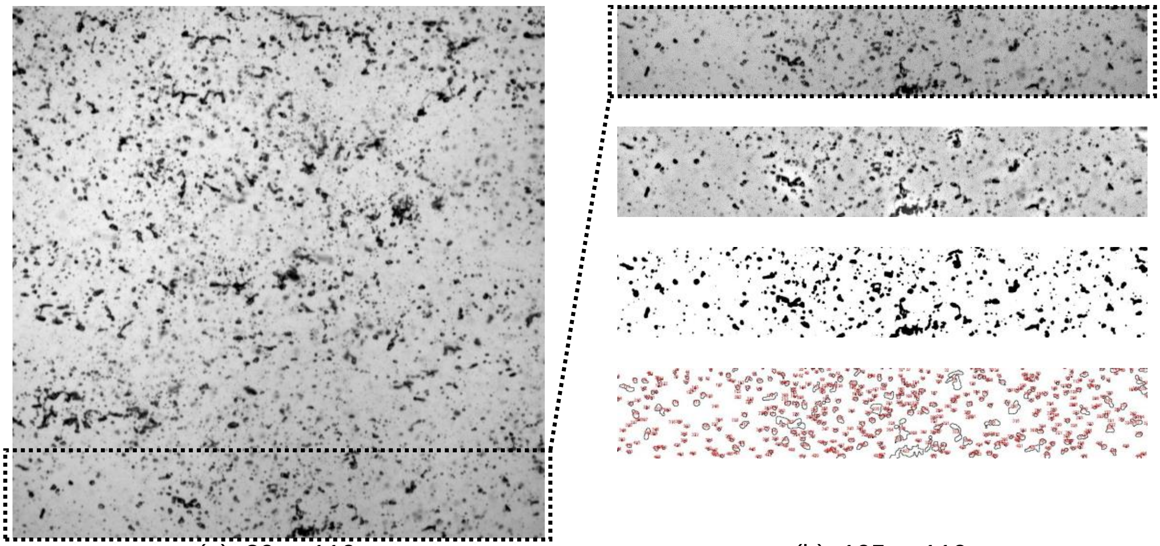

(a) 80 to 110 mm (b) 105 to 110 mm

Figure 6. (a) Shadowgraph of 2,068 kPa water spray; 80 to 110 mm below the nozzle (b) Image processing steps, from top to bottom; 105 to 110 mm below the nozzle.

## Conclusion

A combination of physical and CFD modelling was used to study a flat fan water spray with application in metal powder production. The experimental study involved high-speed shadowgraph imaging of the spray along with image post processing to obtain information about the spray including spreading angle, dispersion angle, and droplet size distribution. The CFD model combines Eulerian and Lagrangian approaches to simulate the continuum phase, air, and discrete phase, water droplets, respectively. The model does not consider the initial water sheet at the vicinity of nozzle and so starts with the injection of water droplets. The initial size distribution of the water droplets is calculated based on the primary break up model developed for a 2D viscous liquid sheet subject to aerodynamic instabilities. A further break up of parent droplets to child droplets is simulated using a secondary break up model. The CFD model provides information about size distribution and velocity of droplets. A benchmark spray at 2,068 kPa pressure was imaged and subsequently modelled. The predicted spray is qualitatively in agreement with the experiment, i.e. in terms of spray pattern. However, the quantitative check on the droplet size distribution suggests that the model requires develoopment. The CFD model yields narrower spread droplet size distribution than the experimental result. This is believed to be due to one or some of the following:

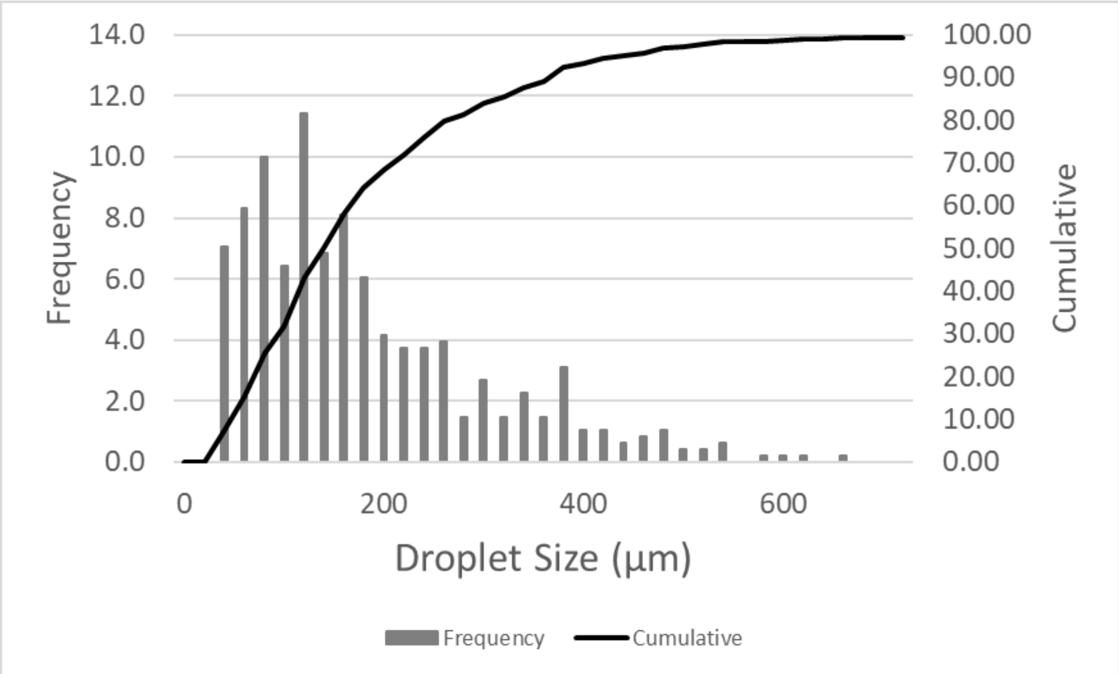


(a) 80 to 110 mm

Figure 7. Droplet size distribution corresponding to Figure 6(b). Arithmetic mean diameter ($d_{10}$) = 178 μm.

(i) the atomization model which was originally developed for pressure-swirl atomizers (ii) strong turbulence in the experimental flat fan nozzle which is not accounted for in the model, and (iii) the secondary break-up model which might not work best for this type of spray or range of pressures. Further investigation on this topic is ongoing. Once the model is further refined it can provide more information on water sprays in metal atomization applications, which, in turn, contributes to understanding and controlling as-atomized powder characteristics.

**References**

[1] Metal Powder Industries Federation (n.d.) Powder Metallurgy—Intrinsically Sustainable. Retrieved February 01, 2018, from https://www.mpif.org/IntroPM/PDFs/PM-Intrinsically-Sustainable.pdf

[2] Pease, L. F. (1983). An Assessment of Powder Metallurgy Today and Its Future Potential. SAE Technical Paper Series. doi:10.4271/831042

[3] Metal Powder Industries Federation. (2017) Powder Metallurgy Industry Roadmap. Retrieved February 01, 2018, from https://www.mpif.org/MarketPM/roadmap.asp

[4] Neikov, O. D., Murashova, I. B., Yefimov, N. A., & Naboychenko, S. (2009). Handbook of non-ferrous metal powders: technologies and applications. Elsevier.

[5] Persson, F., Eliasson, A., & Jönsson, P. (2012). Prediction of particle size for water atomised metal powders: parameter study. Powder Metallurgy, 55(1), 45-53.

[6] Asgarian, A., Wu, C., Li, D., Bussmann, M., Chattopadhyay, K., Lemieux, S., Girard, B., Lavallee, F., & Paserin, V. (2018). Experimental and Computational Analysis of a Water Spray; Application to Molten Metal Atomization. To be published in Advances in Powder Metallurgy & Particulate Materials.

[7] Senecal, P. K., Schmidt, D. P., Nouar, I., Rutland, C. J., Reitz, R. D., & Corradini, M. L. (1999). Modeling high-speed viscous liquid sheet atomization. International Journal of Multiphase Flow, 25(6-7), 1073-1097.

[8] Taylor, G. I. (1963). The shape and acceleration of a drop in a high speed air stream. The scientific papers of GI Taylor, 3, 457-464.

[9] Beale, J.C., and Reitz, R.D. (1999). Modeling Spray Atomization with the Kelvin-Helmholtz/ Rayleigh-Taylor Hybrid Model". Atomization and Sprays, 9, 623-650.

[10] The OpenFOAM Foundation Ltd., OpenFOAM Version 5.0, 2018. [Online]. Available: www.openfoam.org.